Electronic Supplementary Material (ESI) for Nanoscale.
This journal is © The Royal Society of Chemistry 2017

# Ultralow friction of ink-jet printed graphene flakes

R. Buzio[a]*, A. Gerbi[a], S. Uttiya[a,b], C. Bernini[a], A. E. Del Rio Castillo[c], F. Palazon[d], A. S. Siri[a,b], V. Pellegrini[c], L. Pellegrino[a], and F. Bonaccorso[c]*

[a]*CNR-SPIN Institute for Superconductors, Innovative Materials and Devices, C.so Perrone 24, I-16152 Genova, Italy*
[b]*Physics Department, University of Genova, Via Dodecaneso 33, I-16146 Genova, Italy*
[c]*Istituto Italiano di Tecnologia, Graphene Labs, Via Morego 30, I-16163 Genova, Italy*
[d]*Istituto Italiano di Tecnologia, Nanochemistry Department, Via Morego 30, I-16163 Genova, Italy*

*E-mail: renato.buzio@spin.cnr.it; francesco.bonaccorso@iit.it

# SUPPLEMENTARY INFORMATION

## S1. Applicability of the Maugis-Dugdale continuum model to the tip-flake junction

In the present study, the non-linear friction-load dependence of experimental $F_{fric}$ *vs* $F_N$ curves is traced back to a sublinear increase of the contact area $A$ with the normal load $F_N$, which in turn reflects the reversible elastic deformation of the sphere-on-flat contact geometry. Hence, friction force is assumed to scale linearly with contact area, $F_{fric} = \tau A$, with τ being the interfacial shear strength. This assumption is commonly done to exploit single-asperity contact mechanics in the analysis of atomic force microscopy (AFM) friction force data.[1] Notably, continuum models can effectively interpolate experimental $F_{fric}$ *vs* $F_N$ curves for different carbon-based surfaces, including graphite, micromechanical cleavage (MC) few-layer graphene (FLG) flakes and multilayer graphene thin films,[2-7] and they can provide reasonable estimates for the contact parameters. The use of the Maugis-Dugdale (MD) model appears therefore particularly convenient. Atomistic simulations of *simplified* model systems however show that continuum contact mechanics does not always capture the rich phenomenology of mechanical interactions taking place in nanosized contacts.[8] Hence the MD continuum model, albeit of widespread use, is intended to provide an oversimplified picture of the actual mechanical interactions between the AFM tip and single layer graphene (SLG)/FLG flakes. In particular the assumption $F_{fric} = \tau A$ can break-down at the nanoscale. Hereafter, we resume for completeness two scenarios that invoke incommensurate contacts, rather than $F_{fric} = \tau A$, to explain the sublinear friction-load dependence observed in AFM experiments. Both might be in principle considered to interpret the experimental friction-load curves, even if the complexity of the studied system - tentatively depicted in the sketch of Fig. 7(c) - does not allow gaining deeper knowledge on this aspect.

The first scenario assumes the tip-graphene junction to behave as a rather incommensurate contact due to the amorphous character of the AFM tip. Atomistic simulations indicate that a bare incommensurate contact (with negligible adhesion) exhibits almost no friction,[8] a condition known as superlubricity or structural lubricity. In such case the friction force increases *linearly* with normal load. The assumption $F_{fric} = \tau A$ no longer holds because the contact is atomically rough, being dominated by the inherent, interfacial atomic roughness.[8,9] Van der Waals adhesion is shown to change the $F_{fric}$ *vs* $F_N$ dependence from linear to sublinear, which is consistent with the MD model and qualitatively agrees with AFM experiments.[9] However, material parameters within the contact region are not properly captured when interpolating such simulations with the MD model.[9] It follows that sublinear friction-load curves have to be explained through a complex interplay of adhesion and atomic roughness effects, rather than through $F_{fric} = \tau A$. Very recent simulations indicate that a comprehensive treatment of the tip-flake junction should also account for the graphene out-of-plane flexibility, as this drives the contact area and the interfacial friction to evolve continuously under applied strains *via* atomic configurational relaxations.[10]

The second scenario assumes that incommensurability at the tip-graphene contact might be caused by a small graphene flake at the tip apex, forming an incommensurate contact with the underlying graphene surface. This picture follows from well-known AFM experiments on graphite,[11] in which peculiar atomically-resolved friction maps were interpreted assuming that a graphite flake was dragged along with the tip and the friction between a graphene flake and the remaining graphite sheet was measured instead of that between the tip and graphite. For such an extended contact, the friction force strongly depends on the orientation of the flake with respect to the substrate. The two contacting surfaces form a superstructure with a Moiré pattern, which gives the relevant friction force. In particular for angles in between commensurate conditions, the potential barriers to sliding are averaged out leading to structural lubricity. Structural lubricity is nonetheless reversible

disrupted at certain values of normal load, so that non-linear $F_{fric}$ *vs* $F_N$ curves can be ascribed to a progressive locking and commensurability transition of the tip flake, as a result of vertical motion of its edge atoms.[12] Again the assumption $F_{fric} = \tau A$ does not strictly hold for a flake mediated tip-graphene contact. As in the present experiment nanosized liquid phase exfoliation (LPE) flakes are studied, one cannot exclude that small flakes might be occasionally captured by the AFM tip apex.

## S2. Morphology, adhesion and friction of LPE nanoflakes drop-casted onto $SiO_2$

Figure S1 resumes typical AFM morphology, friction and adhesion data for an individual FLG flake produced by LPE of pristine graphite in N-methyl2pirrolidone (NMP), belonging to the sample prepared by drop-casting onto $SiO_2$ (see sect.2.3 and 2.4 of the main text for details). When imaging individual flakes, $F_N$ is in the range of a few nN, to avoid tip-induced translation and edge wear (see also sect. 3.4. of the main text).

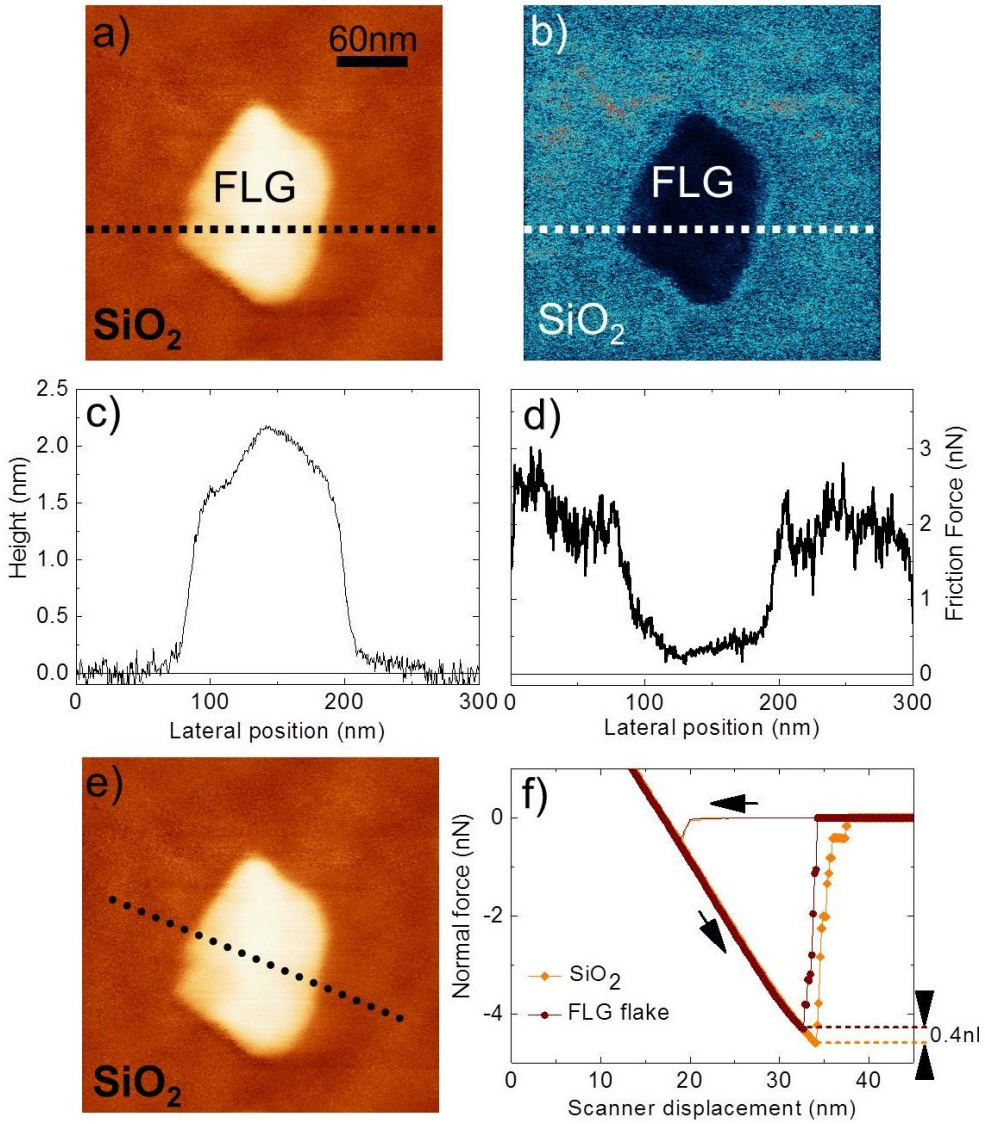


**Figure S1** (a),(b) Topography and friction maps acquired simultaneously on a FLG nanoflake deposited on $SiO_2$ ($F_N$ ~5.1nN). (c),(d) Scan lines corresponding to dash lines in (a) and (b) respectively. They confirm the significant reduction of friction for the ~2nm-thick flake. (e) Individual normal force vs displacement curves are acquired across the flake at the in-plane positions indicated by the black circles. Curves on FLG and $SiO_2$ are separately averaged and reported in (f). The pull-off force on FLG is reduced by ~0.4nN compared to that on $SiO_2$.

## S3. Normal force spectroscopy for FLG printed on HMDS-$SiO_2$

Figure S2 resumes normal force spectroscopy data for FLG printed onto HMDS-$SiO_2$. Briefly, the pull-off (adhesion) force on printed FLG is smaller, or at most comparable, with that measured on the deposition substrate.

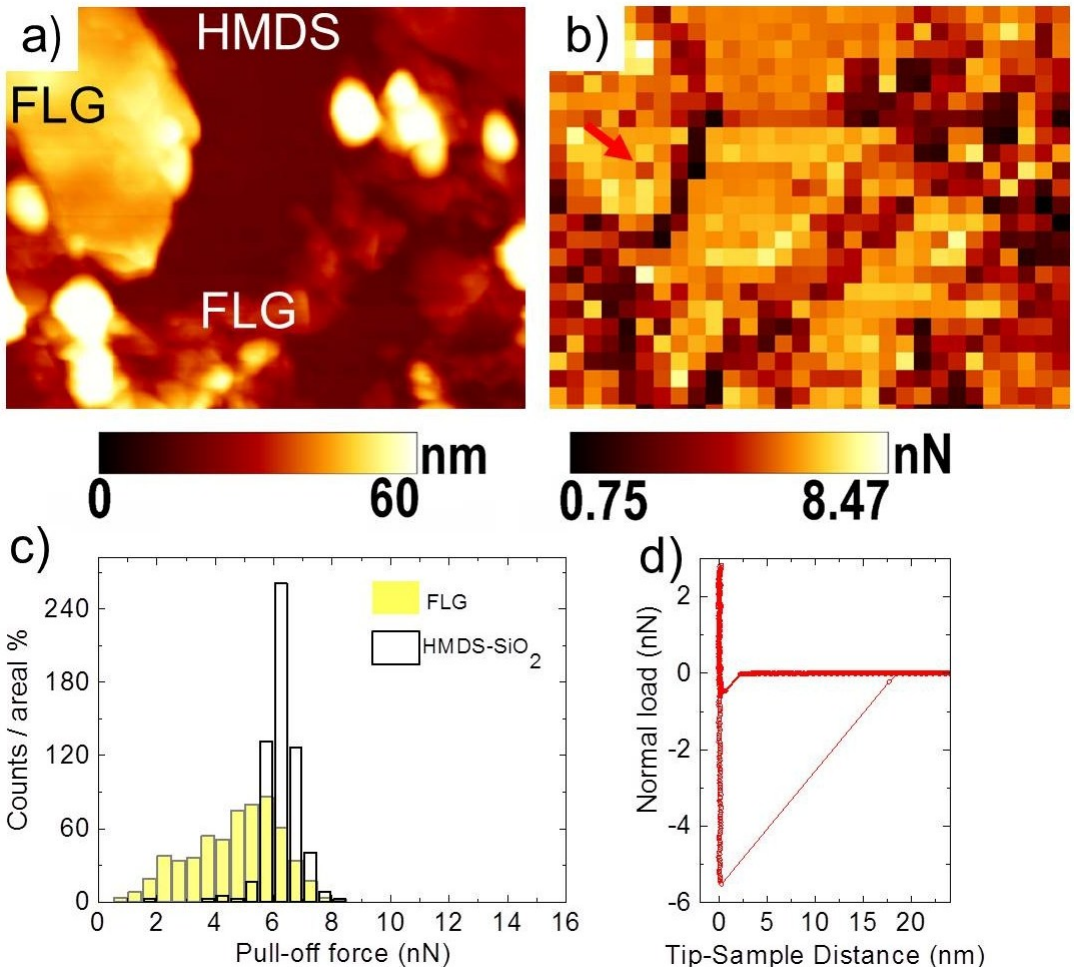


**Figure S2** (a) Topography of FLG printed onto HMDS-$SiO_2$ (size 2.0×1.5μm$^2$). (b) Pull-off force map measured on the aggregate in (a), showing reduced adhesion on FLG with respect to the deposition substrate. (c) Histogram of pull-off forces from the map in (b). (d) Force-distance curve acquired on printed FLG, at the spot indicated by the red arrow in (b). Force profile corresponds to the formation of a mechanically-stiff tip-FLG junction.

## S4. Friction response of the HMDS – $SiO_2$ surface

Figure S3 reports representative friction *vs* load curves acquired sequentially over the same surface region of the HMDS-$SiO_2$ substrate. With respect to the characteristics in Figure 6(a), the normally-applied load is here increased from snap-in-contact (~0nN) up to 32nN. A broad friction bump appears above 20nN in scan #1 and shifts towards lower loads in the successive scans (~18nN in #2, ~15nN in #3 and ~12nN in #4). As a result, curves #1 and #4 look substantially different for loads above 12nN. This evolution indicates mechanical instability of the tip-sample junction. This is confirmed by observation of wear debris in the topographies acquired after the scans.

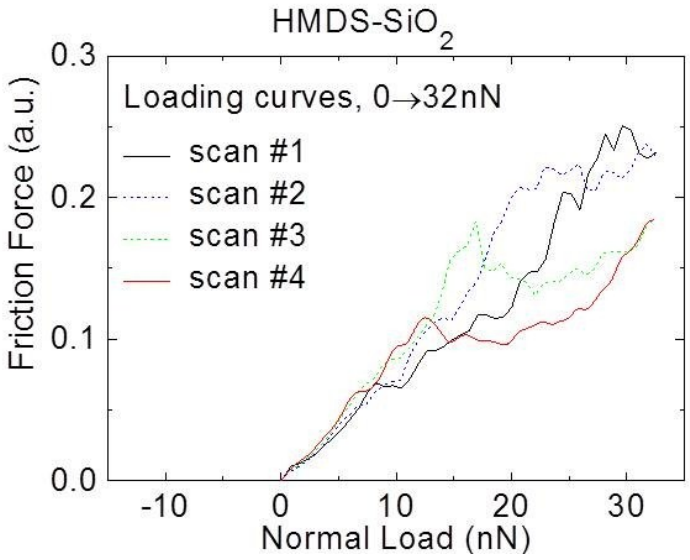


**Figure S3** Evolution of friction *vs* load characteristics (#1….#4) acquired sequentially over the same surface spot.

## S5. Friction response of micromechanically cleaved SLG/FLG

We prepared reference samples of SLG and FLG by MC of graphite on $SiO_2$ substrates. To this purpose we used highly oriented pyrolytic graphite HOPG (ZYB quality by NT-MDT, Russia).

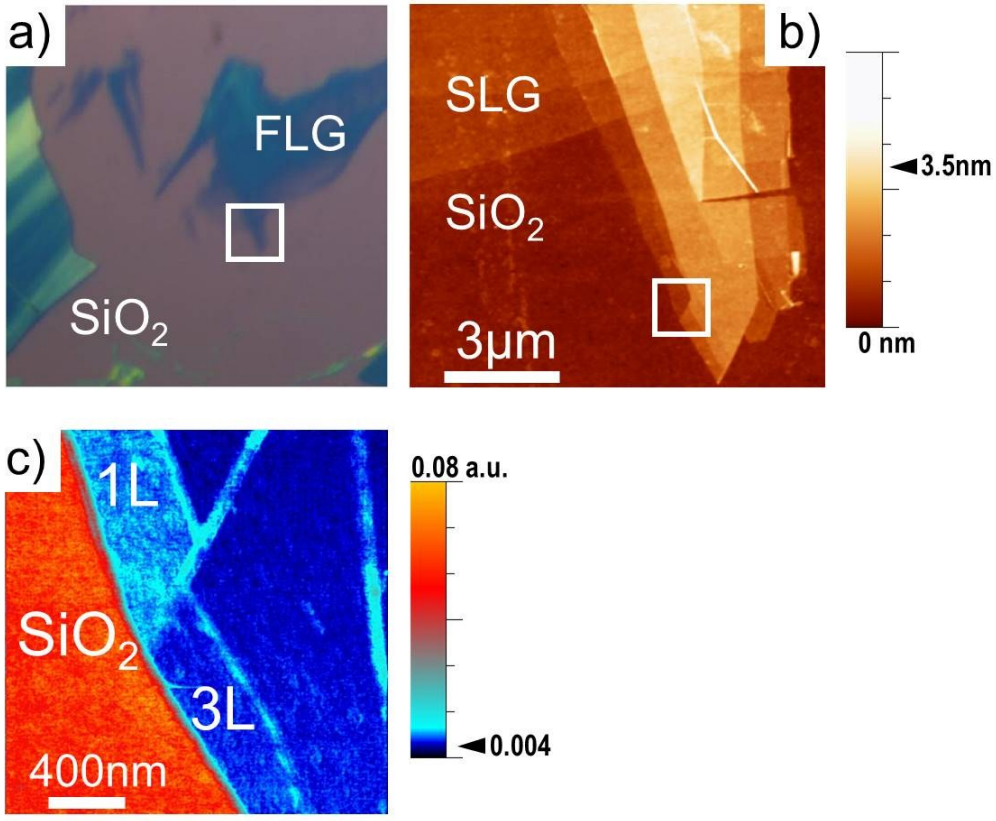


**Figure S4** (a) Optical image of FLG mechanically exfoliated onto $SiO_2$. (b) AFM topography corresponding to the region highlighted in (a), revealing the atomic steps of individual graphene layers. (c) Friction map for the region highlighted in (b). It shows a large friction contrast between $SiO_2$ and graphene, together with thickness-dependent friction for FLG. In fact, friction is clearly higher on the mono-layer (1L) area compared to the tri-layer (3L) region.

After deposition, the thinnest flakes were first identified with optical microscopy, see Figure S4 (a). These flakes have typical lateral dimensions of tens of micrometers. Their thicknesses and friction were systematically measured by AFM. Figure S4 resumes data for a region containing thin and thick flakes.

## S6. Properties of *O*DCB - based FLG ink

The morphology of the flakes produced by LPE of pristine graphite in ortho-dichòorobenzene (*O*DCB) is characterized by TEM (see Figure S5(a) where a representative TEM bright field image is reported). The TEM images allow the estimation of the lateral size of the flakes, with the statistical analysis that shows a main lateral size distribution centred at ~150 nm (Figure S5(a)).

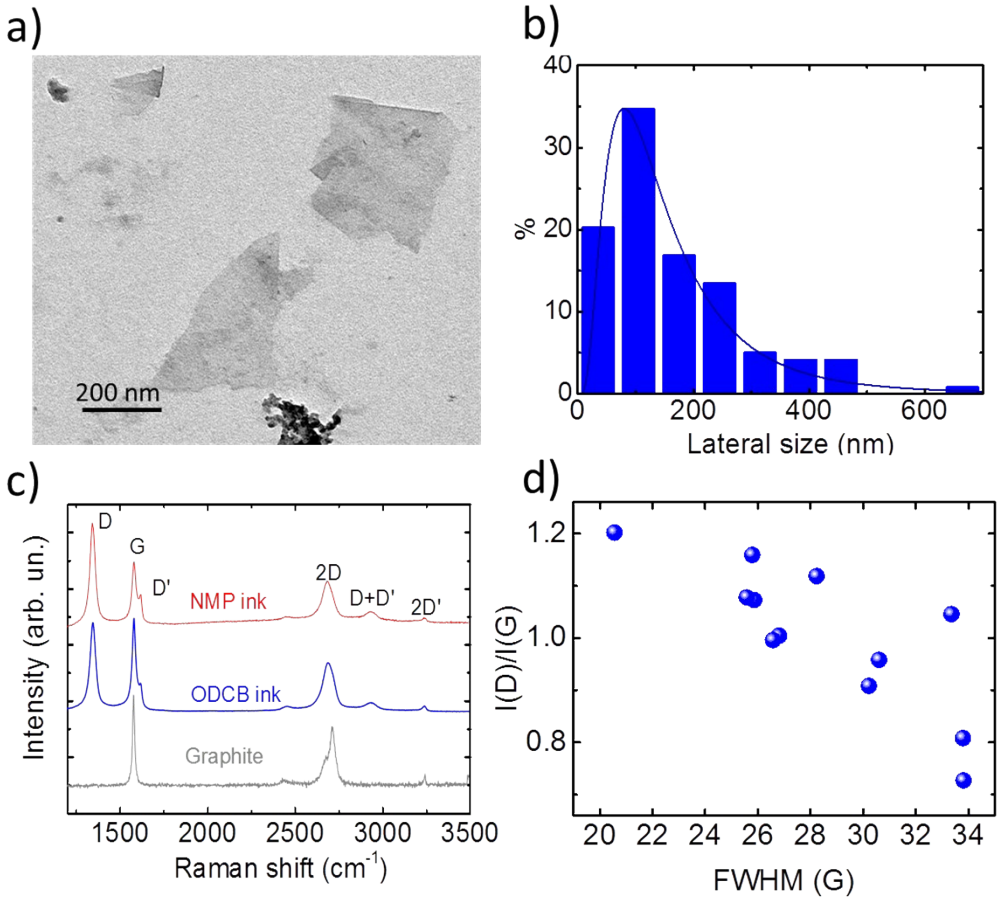


**Figure S5.** (a) Transmission electron microscopy of FLG flakes exfoliated in ODCB and (b) the statistical lateral size distribution. (c) Raman spectrum of the ink in ODCB (blue curve). The Raman spectra of the NMP exfoliated sample (red curve) and the starting graphite (grey curve) are also shown for comparison. (d) The I(G)/I(D) ratio plotted against the FWHM (G) shows no correlation, indicating that the defects are edges rather than structural in-plane.

The Raman spectrum of the as-prepared ink (Figure S5(c)) as well as the spectra of the starting material, *i.e.*, graphite, and the ink in NMP are shown for comparison. The 2D peak gives us information about the number of layers. An estimation of the thickness of the sample can be made by evaluating the $2D_1/2D_2$ ratio, which in our case indicates that our ink is enriched with FLG. The Raman spectrum of the ink produced in *O*DCB also shows significant D and D' intensity, with an average intensity ratio I(D)/I(G)~1, Figure 1 S5(c). This is attributed to the edges of our sub-micrometer flakes, rather than to the presence of basal plane structural defects in the flakes. This observation is supported by the lack of a linear correlation between I(D)/I(G) and FWHM(G). In fact, by combining I(D)/I(G) with FWHM(G) allows us to discriminate between disorder localized

at the edges and disorder in the bulk. In the latter case, a higher I(D)/I(G) would correspond to higher FWHM(G). Figure S5(d) shows that I(D)/I(G) and FWHM(G) are not correlated, an indication that the major contribution to the D peak comes from the sample edges.

## S7. Friction response of *O*DCB-based graphene ink

We probed the friction of FLG printed onto bare $SiO_2$ and HMDS-$SiO_2$, starting from an *O*DCB-based ink. Figure S6 reports a representative, average friction *vs* load characteristic. Interpolation with the MD model gives a shear stress $\tau = 44 MPa$ , not far from that measured for the NMP-based graphene inks (see also Table 1 in the main text). A curvature radius R=20nm is used for the calculation.

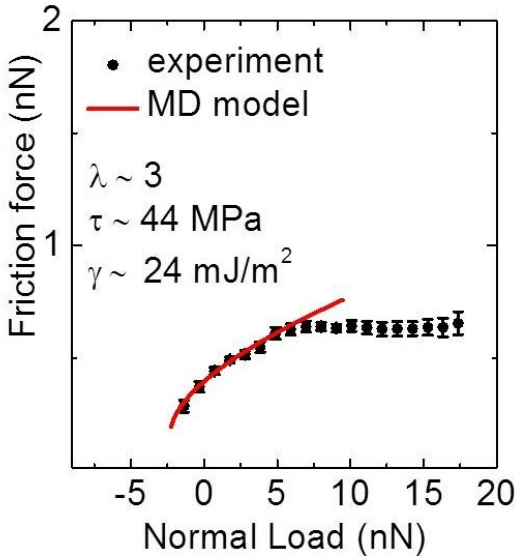


**Figure S6** Average friction *vs* load curve acquired on printed FLG deposited from *O*DCB ink (average over 10 individual curves).

## S8. X-ray photoelectron spectroscopy

For detailed analysis about the presence of nitrogen, we carried out the X-ray photoelectron spectroscopy (XPS) N 1s spectra of the deposited samples before and after annealing. The total area of the XPS N 1s core-level spectra of the LPE FLG is normalized by the relative nitrogen amount (N/(N+C)). The nitrogen relative amount is reduced by ca. 35% upon annealing, accompanied by a decomposition of NMP[13] as can be seen by the appearing of a second component at lower binding energy, see Figure S7.

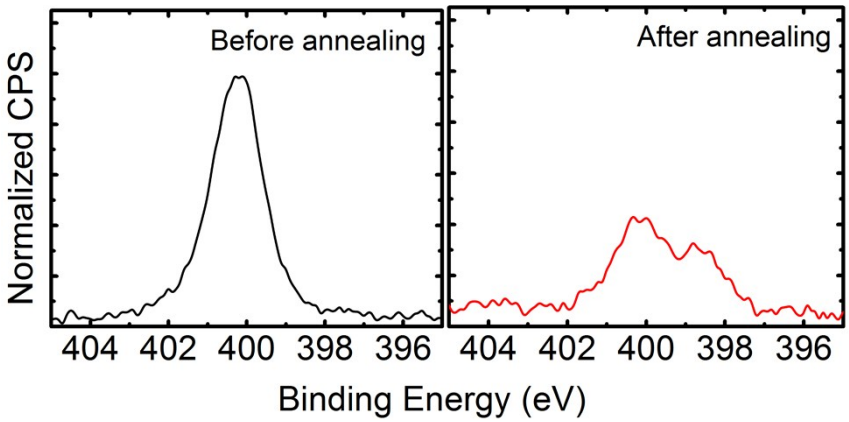


**Figure S7.** The XPS N 1s core-level spectra of the LPE FLG before and after annealing at 350°C in high vacuum.

## S9. Friction of printed FLG vacuum annealed at T≤250°C

Following literature data,[14] we carried out experiments to remove the solvent contamination from printed FLG flakes by 10 up to 60 minutes vacuum-annealing at temperatures T≤250°C. Friction maps demonstrated that such treatment was insufficient to remove solvent molecules from the FLG flakes surface. In fact, under such condition only a fraction of the FLG flakes – as identified from the topographical maps – displayed ultralow friction. The situation is exemplified in Figure S8 for the case of NMP-based ink printed on HMDS-$SiO_2$.

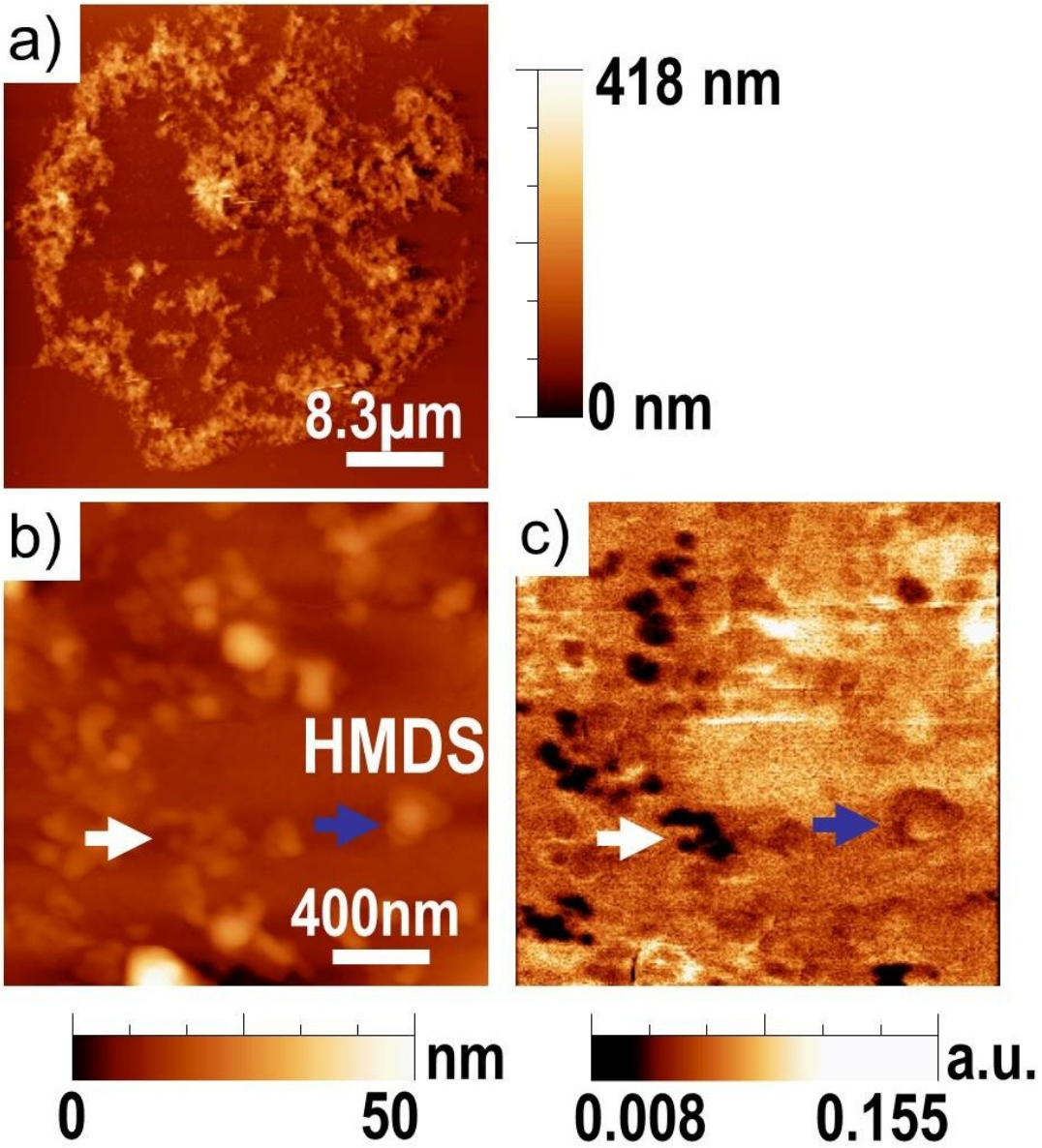


**Figure S8** (a) A FLG microdrop inkjet printed on HMDS-$SiO_2$ using the NMP-based ink and annealed for 10minutes at 170°C. (b) AFM topography and (c) friction maps for a selected region, attesting friction heterogeneity. The white arrow highlights a group of FLG flakes with ultralow friction. The blue arrow on the contrary shows that there are flakes with friction comparable with the deposition substrate. This behaviour reflects massive surface contamination by residual NMP.

## S10. Friction at the printed FLG edges

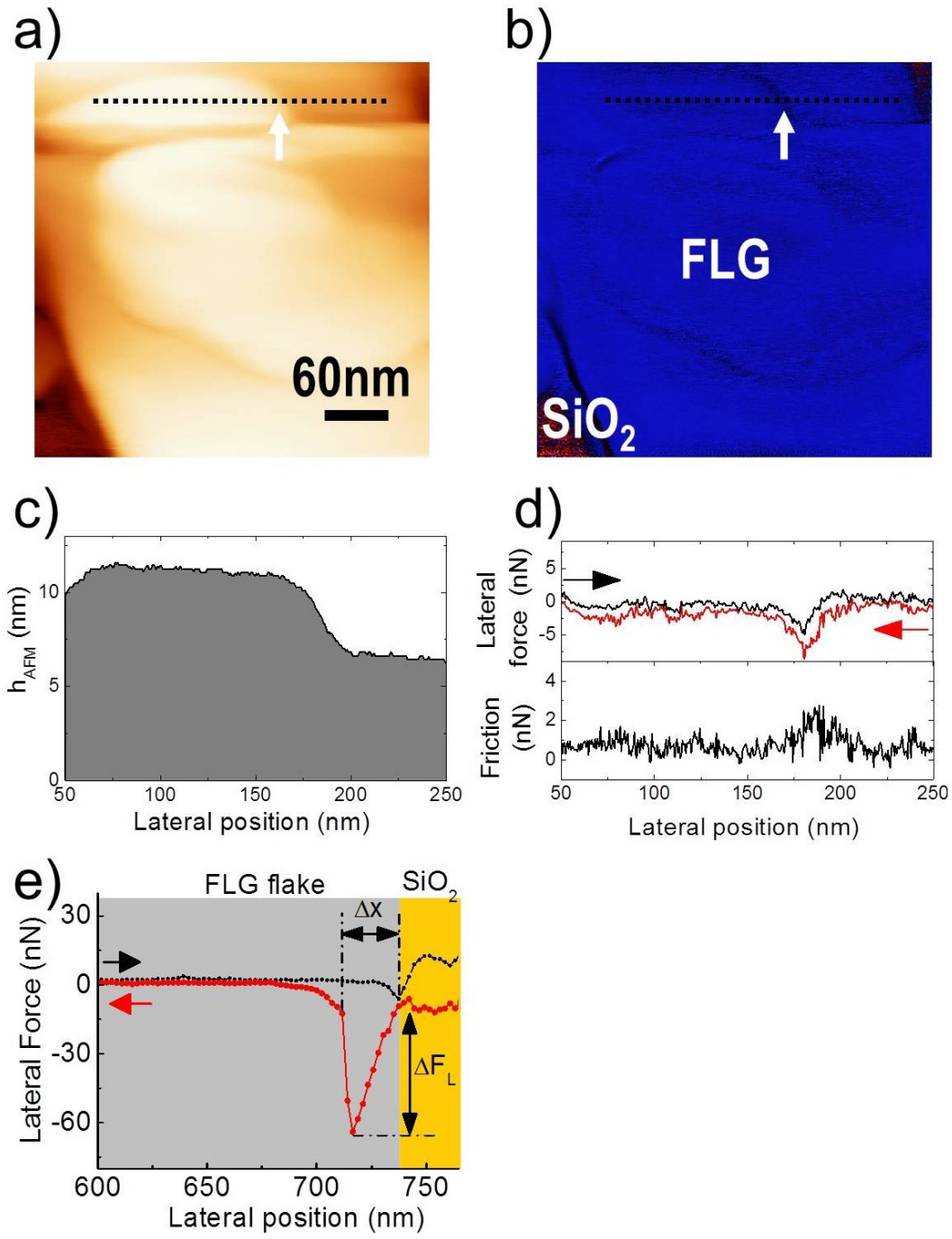


**Figure S9** (a) Topography and (b) lateral force maps for a printed aggregate formed by stacked FLG flakes. A surface exposed step edge is highlighted by the white arrow. (c) Height profile along the dash line in (a) and (b), showing the step edge at the lateral positions between 175nm and 200nm. (d) Lateral force and friction profiles along the dash line reported in (a) and (b), respectively. A friction spike occurs at the position of the step edge. (e) Magnification of the lateral force profile shown in Fig. 8(d) of the main text.

The stick-slip spike in Figure S9(e) has a width $\Delta x$~30nm and amplitude $\Delta F_L$~55nN. The effective spring constant for flexing the FLG edge, estimated from the linear response of the lateral force, is ~1.8N/m. This value is nearly 16 times smaller than the torsional spring constant of the AFM probe $k_{tip} = GJ/[l(h+t/2)2] \approx 29$ N/m, where G = 64GPa is the shear modulus of silicon, J is the torsion constant (approximated as $0.3wt^3$, where w is the 35μm width and t is the 2μm thickness of the

cantilever), *l* is the 350μm length of the cantilever, and *h* is the 22μm height of the tip apex. Hence, the majority of the deflection Δx occurs within the FLG flake when the tip is laterally pressed against its edge at position B.
The effective spring constant of ~1.8N/m overcomes by a factor 6 to 9 that reported for MC SLG (0.2N/m - 0.3N/m). We believe that force increase might reflect, in the present case, elastic straining of more than one graphene layers.

# References


1. I. Szlufarska, M. Chandross, R.W Carpick, *J. Phys. D: Appl. Phys.* 2012, **41**, 123001
2. Z. Deng, N. N. Klimov, S. D. Solares, T. Li, H. Xu and R. J. Cannara, *Langmuir*, 2013, **29**, 235–43.
3. H. Chen and T. Filleter, *Nanotechnology*, 2015, **26**, 135702.
4. R. Buzio, C. Boragno and U. Valbusa, *J. Chem. Phys.*, 2006, **125**, 094708.
5. R. Buzio, E. Gnecco, C. Boragno and U. Valbusa, *Carbon N. Y.*, 2002, **40**, 883–890.
6. R. Buzio, C. Boragno and U. Valbusa, *Wear*, 2003, **254**, 981–987.
7. Z. Deng, A. Smolyanitsky, Q. Li, X.-Q. Feng and R. J. Cannara, *Nat. Mater.*, 2012, **11**, 1032–7.
8. B. Luan, M.O. Robbins, *Nature,* 2005, **435**, 929-932.
9. Y. Mo, K.T. Turner, I. Szlufarska, *Nature,* 2009, **457**, 1116-1119.
10. S. Li, Q. Li, R.W. Carpick, P. Gumbsch, X. Z. Liu, X. Ding, J. Sun, J. Li, *Nature*, **2016**, 539, 541-546.
11. M. Dienwiebel,G.S. Verhoeven, N. Pradeep, J.W.M. Frenken, J.A. Heimberg, H.W. Zandbergen, *Phys. Rev. Lett.*, **2004**, 92, 126101-1/4.
12. M. M. van Wijk, M. Dienwiebel, J. W. M. Frenken, and A. Fasolino, *Phys. Rev. B*, **2013**, **88**, 235423-1/6.
13. H. C. Yau, M. K. Bayazit, J. H. G. Steinke and M. S. P. Shaffer. *Chem. Commun*., 2015, **51**, 16621-16624.
14. F. Torrisi, T. Hasan, W. Wu, Z. Sun, A. Lombardo, T. S. Kulmala, G.-W. Hsieh, S. Jung, F. Bonaccorso, P. J. Paul, D. Chu and A. C. Ferrari, *ACS Nano*, 2012, **6**, 2992–3006.